

Measurement of the $2S_{1/2} - 8D_{5/2}$ transition in hydrogen

A. D. Brandt, S. F. Cooper, C. Rasoar, Z. Burkley,* and D. C. Yost†
Department of Physics, Colorado State University, Fort Collins, CO 80523

A. Matveev

Russian Quantum Center, Skolkovo, Moscow 143025, Russia

(Dated: November 19, 2021)

We present a measurement of the hydrogen $2S_{1/2} - 8D_{5/2}$ transition performed with a cryogenic atomic beam. The measured resonance frequency is $\nu = 770649561570.9(2.0)$ kHz, which corresponds to a relative uncertainty of 2.6×10^{-12} . Combining our result with the most recent measurement of the $1S-2S$ transition, we find a proton radius of $r_p = 0.8584(51)$ fm and a Rydberg constant of $R_\infty = 10973731.568332(52)$ m⁻¹. This result has a combined 3.1σ disagreement with the CODATA 2018 recommended value. Possible implications of the discrepancy are discussed.

Spectroscopy of hydrogen, the simplest element, was pivotal in the development of quantum theory and now plays a crucial role in the determination of fundamental constants and precision tests of fundamental theory [1–3]. Due to its simplicity, theoretical calculations of the energy levels of hydrogen can be made with high accuracy, and deviations from theoretical predictions could suggest the presence of new physics [4–8].

The energy levels of hydrogen can be described by the following expression, given by [9, 10],

$$E_{n,l,j} = hcR_\infty \left(-\frac{1}{n^2} + f_{n,l,j}(\alpha, \frac{m_e}{m_p}, \dots) + \delta_{l,0} \frac{k_N}{n^3} r_p^2 \right). \quad (1)$$

The first term, which depends only on the principle quantum number n , is the gross structure contribution from nonrelativistic quantum theory. The second term accounts for quantum electrodynamics (QED) and relativistic recoil corrections [3, 11]. The last term is the leading correction to the S states arising from the finite size of the nucleus, where r_p is the root-mean-square charge radius of the proton. By measuring two hydrogen transitions, the Rydberg constant, R_∞ , and r_p in Eqn. (1) can be determined. While $f_{n,l,j}$ is a function of other physical constants, such as the fine-structure constant and electron-to-proton mass ratio, each of these have been measured with sufficient precision in other experiments to not limit the determination of R_∞ and r_p . Therefore, assuming that the QED corrections are accurately applied, a consistent extraction of R_∞ and r_p from spectroscopic measurements is expected.

Tension arose when the value of r_p obtained from muonic hydrogen was compared to the value determined from hydrogen spectroscopy and electron-proton elastic scattering data. This led to the “proton-radius puzzle” [12–15]. This discrepancy has spurred further interest in precision spectroscopy on hydrogen, and several new results have been recently published [9, 10, 16, 17].

The CODATA 2014 recommended r_p value, which is historically significant in the discussion of the proton-radius puzzle, is strongly influenced by previous measure-

ments of the two-photon $2S-8S/D$ transitions [18, 19]. While remeasuring any of these transitions produces data relevant to the proton radius puzzle, the $2S_{1/2}-8D_{5/2}$ transition is particularly attractive as it possesses the largest two-photon matrix element. Therefore, we have remeasured the $2S_{1/2} - 8D_{5/2}$ transition and report a value that has a three-times smaller uncertainty as compared with the previous best measurement [19].

Our measurement has benefited from several technological advances. Improvements in laser technology afford us both the optical frequency comb to determine absolute optical frequencies, and the ability to optically excite a sufficient population of hydrogen atoms to the metastable $2S$ state, as in [9]. By generating metastable atoms optically via the two-photon $1S_{1/2}-2S_{1/2}$ transition, instead of by electron bombardment, we are able to perform spectroscopy on a cryogenic beam of hydrogen atoms, reducing velocity-dependent systematics and allowing for the selective population of the $2S_{1/2}^{F=1}$ hyperfine manifold. Therefore, optical production of an appreciable flux of metastable hydrogen represents a substantial improvement over previous measurements of this transition. We have also directly characterized the velocity distribution, reducing uncertainty in velocity-related systematics [20]. Additionally, our apparatus provides a geometrically-constrained interaction between the hydrogen atoms and the spectroscopy light.

Our experimental apparatus has not been fully described elsewhere. We generate a cryogenic beam of hydrogen by disassociating molecular hydrogen in a microwave discharge followed by a cryogenic nozzle [20]. At a distance of 1.5 m away from the nozzle, the atoms interact with 243 nm radiation to generate $2S_{1/2}^{F=1}$ population. The 243 nm radiation [21] is enhanced in an in-vacuum optical cavity [22] at a 6° angle from the atomic beam. The UV cavity mirrors are kept in a ~ 200 mTorr oxygen environment to prevent UV degradation, and a pair of differential pumping manifolds separates the mirror chambers from the spectroscopy region. The metastable $2S$ atoms then travel 15 cm before intersecting with 778 nm spectroscopy light from a Coherent-899 Ti:Sapphire

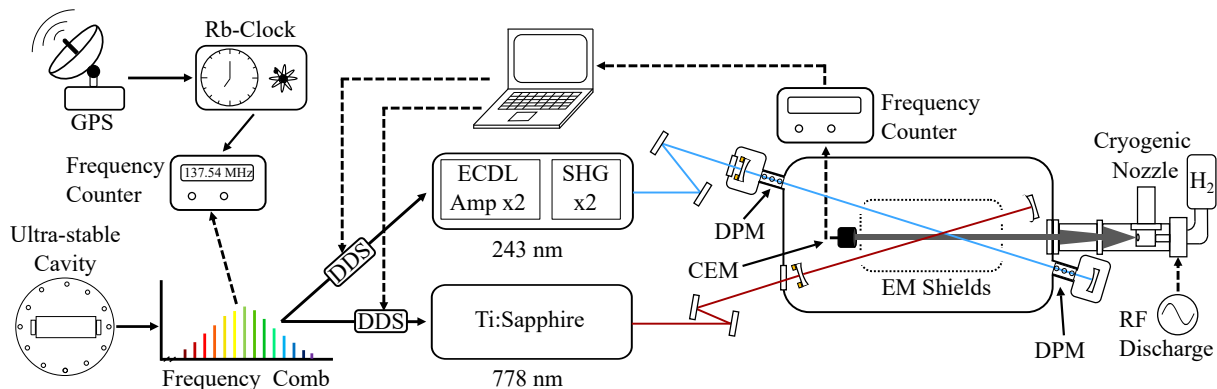


FIG. 1. Schematic of experiment. The repetition rate of the coherent frequency comb referenced to an ultra-stable optical cavity is counted by a GPS-disciplined Rubidium time standard. The 243 nm and 778 nm lasers are phase-locked to the comb, with the beat frequency set by a direct digital synthesizer (DDS). The Ti:Sapphire laser is a Coherent-899 vertically oriented ring laser with a modified piezoelectric controlled mirror to increase the frequency locking bandwidth. ECDL: Extended cavity diode laser. SHG: Second-harmonic generation. DPM: Differential pumping manifolds. CEM: Channel electron multiplier. EM Shields: A pair of coaxial magnetic shields within a Faraday cage.

ring laser, which is also enhanced in an in-vacuum optical cavity at a 6° angle from the atomic beam. The linearly polarized 778 nm radiation excites the $2S_{1/2}-8D_{5/2}$ transition. Population in the $8D_{5/2}$ state will rapidly decay – predominantly to the $2P$ state which will then decay to the $1S$ ground state. Therefore, by driving the $2S_{1/2}-8D_{5/2}$ transition, we effectively quench the metastable population. The entire spectroscopic volume is within a pair of concentric magnetic shields, which is itself inside of a Faraday cage to mitigate Zeeman shifts and DC Stark shifts. The remaining metastable population not quenched by the 778 nm radiation is detected 15 cm past the $2S_{1/2}-8D_{5/2}$ interaction volume by a channel electron multiplier. The absolute frequencies of the 243 nm and 778 nm radiation are determined by phase-locking the lasers to a coherent Er-fiber optical frequency comb whose repetition rate is continuously counted by a GPS-disciplined, Rb time base and whose f_0 beat note is phase locked to an RF synthesizer. See Fig. 1 for a schematic of our experimental apparatus.

The UV-enhancement cavity is about 1.8 m long and is constructed with a pair of 1 m radius of curvature mirrors – the effective $1/e^2$ beam radius is approximately $150 \mu\text{m}$ at the intersection with the atomic beam. Between 1% and 10% of atoms in the excitation volume are driven to the $2S_{1/2}^{F=1}$ state. The spectroscopy light is also enhanced in an in-vacuum optical cavity to drive appreciable population to the $8D_{5/2}$ state and the optical power is measured by continuously monitoring the cavity transmission with a photodiode.

A direct digital synthesizer (DDS) sets the beat frequencies between the comb and the other laser systems – the DDS itself is referenced to a 10 MHz signal from a GPS-disciplined, Rb time standard. To verify that our absolute frequency calibration is accurate, we locally counted a cesium-referenced 5 MHz signal at the NIST

WWVB station in Fort Collins, Colorado with the Rb-time base and frequency counter, finding an accuracy within the expectations of a GPS-disciplined oscillator [23] (a fractional accuracy of $\approx 5 \times 10^{-13}$).

To scan the $2S_{1/2}-8D_{5/2}$ transition, a set of 25 evenly spaced frequencies in a 3 MHz span around the resonance are chosen. This set of 25 frequency points is randomly sequenced. For each scan of the line, we fit the measured lineshape with

$$\mathcal{F} = A \exp[-\alpha(\mathcal{L}_2(\nu_c, \gamma) + \mathcal{L}_3(\nu_c, \gamma))], \quad (2)$$

where \mathcal{L}_i 's correspond to Lorentzian functions of appropriate relative magnitude centered on the $F = i$ hyperfine manifold, and $\{\alpha, \gamma, \nu_c\}$ are fit parameters for the amplitude of the metastable decrease, linewidth, and effective centroid frequency, respectively. Further details on the fitting function and other possible lineshape distortions (including quantum interference [24]) can be found in the supplementary material (SM).

We have developed numeric lineshape models, which take into account the geometry and dynamics of the atom-light interaction, AC and DC Stark effects, velocity distribution, repopulation of the metastable state, and the second-order Doppler shift (see SM). The numeric models are primarily used to quantify the DC Stark effect, but are also used to verify the accuracy of fitting lineshapes with Eqn. (2).

The AC Stark shift is our leading systematic, with typical shifts in the range of 50-300 kHz. To properly account for this effect, we drive the resonance with a range of intensities, quenching between 15% and 60% of the metastable population, and extrapolate to zero laser power. This extrapolation is similar to previous measurements of the $2S-nS/D$ transitions [19, 25, 26]. For each day of data collection, a single extrapolation is generated (an example is shown in Fig. 2).

The AC Stark effect introduces a shift in the resonance frequency of the $2S_{1/2} - 8D_{5/2}$ transition that is linear with intensity [27]. However, extrapolations on an ensemble of metastable atoms acquire a slight nonlinearity due to the different intensity profiles sampled by metastable atoms with different trajectories. As atoms following trajectories sampling the most intense portions of the 778 nm cavity mode begin to saturate, atoms along trajectories which sample lower intensities begin to contribute relatively more to the determination of the line center. This effect was present in the previous measurement of the $2S_{1/2} - 8D_{5/2}$ transition [19, 26], though the nonlinearity present in our extrapolations is smaller due to the more stringent geometric constraints on the atomic trajectories in our apparatus.

While the nonlinearity is relatively small, ignoring it shifts the extrapolated resonance frequency by several kHz. Sampling an appreciable range of intracavity laser powers is required to properly determine the nonlinearity. From analytic considerations we have found that the nonlinearity acquired due to this spatial distribution is predominantly cubic and that this conclusion does not depend on the metastable spatial distribution (see SM); both of these results are strongly supported by our numeric lineshape models. Seventeen suitable extrapolations form the basis of our data set, and are shown in Fig. 2.

Our second leading systematic is due to the DC Stark effect, which leads to shifts and distortions of the $2S_{1/2} - 8D_{5/2}$ line. We have taken steps to passively mitigate stray fields by enclosing the entire metastable excitation and spectroscopic volume within a Faraday cage coated in colloidal graphite [29]. Due to the near degeneracy of the 8D, 8P, and 8F manifolds, the transition is very sensitive to static fields with shifts of ~ 12 kHz/(V/m)². Higher lying n -manifolds are even more sensitive to the presence of static fields due to the narrower natural linewidths, increasing degeneracy of the states, and larger dipole matrix elements between the states. This makes the line distortions of transitions to higher n -states a sensitive probe of the stray fields [19].

From measurements of the $2S_{1/2} - 12D_{5/2}$ lineshape distortion, we have observed that the stray fields are stable day-to-day as long as the system remains under vacuum, and that the stray field orientation is parallel with the atomic beam. The orientation of the stray field was determined by varying the excitation light polarization and comparing the shift and distortion of the line. Between batches of data collection on the $2S_{1/2} - 8D_{5/2}$ line, the chamber was vented, leaving the possibility of stray field variation within the data set. Therefore, we also measured the electric field strength for each day *in situ* by averaging several $2S_{1/2} - 8D_{5/2}$ scans from a single day and at similar 778 nm laser power. We then fit this averaged line with the numeric model to match the subtle line distortion and extract the stray DC field (see

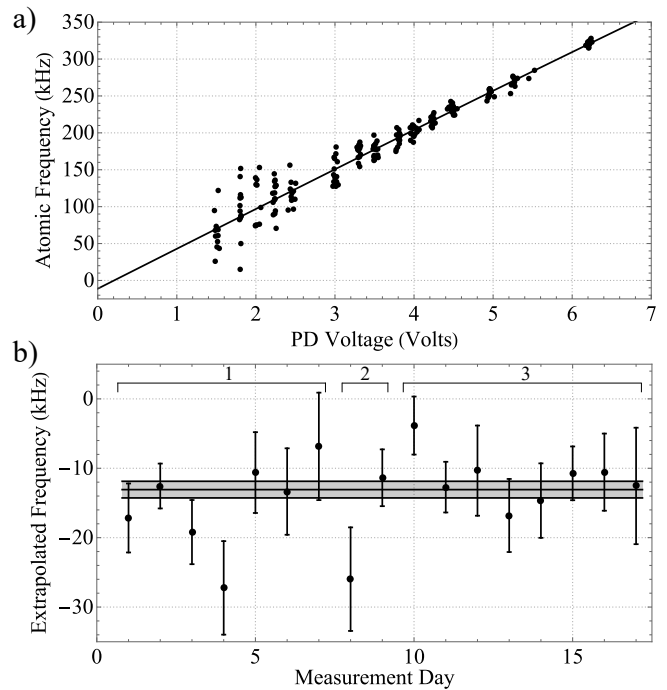


FIG. 2. a) Example AC extrapolation data and cubic fit. b) Extrapolated zero-field frequencies for each measurement day with overall mean and statistical uncertainty overlaid. Data acquisition on the $2S_{1/2} - 8D_{5/2}$ transition was collected in batches grouped by date, which are indicated with batch numbers 1, 2, and 3. Frequencies in both a) and b) are relative to the value listed in [28].

SM for additional detail). Fig. 3 shows the determined electric field for each measurement day. We find the average static field for each batch of data and use that field strength to determine the shift for that set of data.

The coupling introduced by the DC electric field causes a quadratic shift due to nearby dipole-allowed transitions and a lineshape distortion due to the mixing between the nearly degenerate $8D_{5/2}$ and $8F_{5/2}$ states [19]. Since the lines are fit with the simple analytic function given in Eqn. (2), the distortion also produces an additional shift. For each of the three measured electric fields shown in Fig. 3, the resulting DC Stark shift is determined with the numeric model. Then, the appropriate correction for each extrapolated resonance frequency in a given batch is applied. The three batches of electric field corrections are $-1.92(0.32)$ kHz, $-5.45(0.54)$ kHz, and $-4.43(0.37)$ kHz, respectively. Due to the statistical contribution of each batch to the final dataset, the weighted DC Stark correction for the entire measurement is $-3.54(0.37)$ kHz.

The correction of $-3.54(0.37)$ kHz assumes a stray field which is perpendicular to the spectroscopy light polarization. However, we cannot completely exclude a small parallel field, which can modify the required correction by up to 0.65 kHz. Additionally, from the numeric model, we find there is a small amount of cross-talk between the

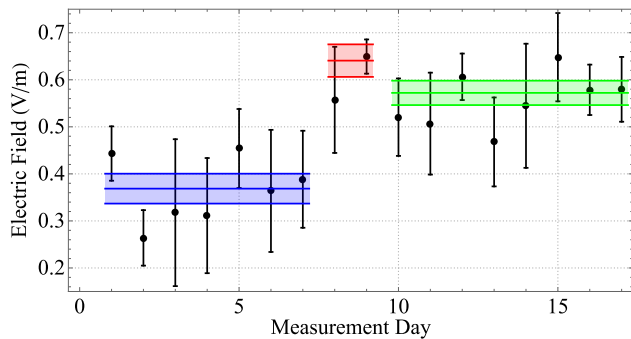


FIG. 3. Fit electric field for each measurement day, with data collection batch average overlaid.

AC extrapolation and DC Stark effect. This cross-talk amounts to a -0.35 kHz correction to the DC Stark shift, and we assign the full 0.35 kHz shift as the associated uncertainty. Since the systematic shifts associated with the cross-talk effect, the possibility of non-perpendicular fields, and the statistical variance of the DC field correction are highly correlated, we combine their uncertainties linearly, and obtain a net DC Stark correction of $-3.89(1.36)$ kHz.

We believe the vacuum pressure is limited by water, which has an intrinsic dipole moment. During a collision with a water molecule, a hydrogen atom experiences a varying electric field which can drive population in the $8D$ state to nearby states, quenching the $8D$ state and broadening the line [30]. We have employed Monte Carlo simulations of these H-H₂O collisions to estimate the shift and broadening, similar to [31]. From these simulations we have found that any associated pressure shifts are below the ~ 1 Hz level and insignificant at our current level of precision.

Due to the two-photon excitation of the $2S_{1/2} - 8D_{5/2}$ transition in an optical cavity, the first-order Doppler shift is effectively absent. The second-order Doppler shift remains, given by $\Delta\nu_{DS} = -0.5(v/c)^2\nu$, for atomic velocity v . An advantage of our apparatus is the ability to directly characterize the hydrogen and metastable hydrogen velocity distributions via a time-of-flight measurement [20]. From such measurements, we have found the metastable velocity distribution is well approximated by $P(v) \propto v^4 e^{-\beta v^2}$, with $\beta = m/2k_bT$ and the required correction is $-0.73(0.10)$ kHz.

From the AC extrapolation data, we recover a $2S_{1/2} - 8D_{5/2}$ hyperfine centroid of $770649561574.90(1.20)$ kHz. The DC Stark correction shifts this centroid by $-3.89(1.36)$ kHz to $770649561571.01(1.82)$ kHz. We then apply minor corrections in our uncertainty budget as shown in Table I. A summary of the treatment of these corrections may be found in the SM. With all the systematic corrections accounted for, we find a $2S_{1/2} - 8D_{5/2}$ resonance

TABLE I. Minor corrections and uncertainties of the extrapolated $2S_{1/2} - 8D_{5/2}$ hyperfine centroid.

	$\Delta\nu$ (kHz)	σ (kHz)
Stark Corrected	770649561571.01	1.82
2 nd Order Doppler	0.73	0.10
Zeeman Effect	0	0.56
Frequency Calibration	-0.40	0.47
Black-body Radiation	-0.49	0.16
Pressure Shifts	0	10^{-3}
$8D_{5/2}$ Hyperfine Structure	0	0.03
Photodiode Imperfections	0	0.32
Incoherent Line Pulling	0	10^{-3}
Light Force Shift	0	10^{-3}
Total: Minor corrections	-0.16	0.82
Hyperfine Centroid	770649561570.9	2.0

frequency of

$$\nu = 770649561570.9(2.0) \text{ kHz.} \quad (3)$$

Combining our result with the $1S_{1/2} - 2S_{1/2}$ value [32], we obtain $r_p = 0.8584(51)$ fm, and $R_\infty = 10973731.568332(52) \text{ m}^{-1}$. Our obtained r_p is presented alongside a selection of recent determinations of r_p from spectroscopic results in Fig. 4. Our value is 3.1 combined standard deviations from the latest CODATA recommended r_p value [33].

While the data shown in Fig. 4 combines the $1S_{1/2} - 2S_{1/2}$ measurement [32] with other hydrogen spectroscopy to extract r_p , it is also interesting to use the value of r_p determined from muonic hydrogen [14] as input data for Eqn. 1. This is a compelling approach considering that a recent measurement of the Lamb shift in normal hydrogen is in agreement with the muonic result

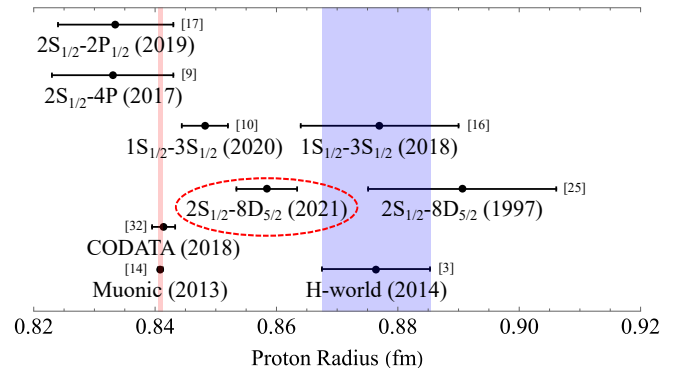


FIG. 4. A selection of recent determinations of the proton radius when combining laser spectroscopy with the $1S_{1/2} - 2S_{1/2}$ transition [9, 10, 16, 26, 32]. The result presented here is circled. The r_p denoted by H-world (2014) corresponds to the proton radius obtained in [3] using only hydrogen spectroscopy data (Adj. 8 Table XXIX). Also shown are the proton radius determinations from Lamb shift measurements in hydrogen [17] and muonic hydrogen [14], along with the most recent CODATA value [33].

[17]. With that, a single measured interval in hydrogen is sufficient to extract R_∞ . The result of this analysis for a selection of the most precise hydrogen laser spectroscopy data is shown in Fig. 5. The uncertainty for the Rydberg constant determination from the $1S_{1/2}$ - $2S_{1/2}$ transition shown in Fig. 5 is almost entirely due to the theoretical uncertainty of the $1S$ state. In order to avoid including this correlated uncertainty in the $1S_{1/2}$ - $3S_{1/2}$ determinations [10, 16], we have subtracted the very precisely determined $1S_{1/2}$ - $2S_{1/2}$ transition frequency [32] to obtain $2S_{1/2}$ - $3S_{1/2}$ intervals.

As can be seen from the Fig. 5, there is a general trend towards larger Rydberg constant when using experimentally determined intervals between states with larger n . It is interesting to note that hydrogen spectroscopy can provide a test for massive bosons that provide an additional coupling between the nucleus and electron [7, 8]. Such bosons introduce a potential with finite range (a Yukawa potential) which affects certain n -states in hydrogen more strongly than others, producing an n -dependence when extracting R_∞ . As shown in the SM, the variation in Rydberg constant tends to decrease as the n of either the upper or lower state increases. We found that the reduced χ^2 for the data shown in Fig. 5 decreases from ~ 4.0 to ~ 2.0 with the addition of a Yukawa potential with a length scale of $\sim 34 a_0$. Therefore, while the perturbation from such a potential can drastically reduce the inconsistency within the dataset shown in Fig. 5, it does not eliminate it.

Future investigations of $2S$ - nS /D transitions in hydrogen are attractive due to the narrow natural lines afforded by such states and the convenience of the laser wavelengths required to drive the transitions. Additionally, the current n -dependence of the Rydberg constant extractions as shown in Fig. 5 provides a compelling case for further measurements of transitions to relatively high n as a search for new physics [7, 8]

We gratefully acknowledge useful conversations with J. Berger, S. M. Brewer, A. Grinin, S. A. Lee, L. Maisenbacher, R. Pohl, J. L. Roberts, Th. Udem, and V. Wirthl. We would like to thank the NIST WWVB team for accommodating our check of the GPS disciplined Rb time standard as described in the letter. Finally we gratefully acknowledge funding for this measurement through the NIST Precision Measurement Grant (60NANB16D270), and the NSF CAREER Award (1654425).

* Now at Dep. Physik, ETH Zürich

† Dylan.Yost@colostate.edu

- [1] S. G. Karshenboim, Precision physics of simple atoms: QED tests, nuclear structure and fundamental constants, *Phys. Rep.* **422**, 1 (2005).
 [2] S. G. Karshenboim, F. S. Pavone, G. F. Bassani, M. Inguoscio, T. W. Hänsch, *Introduction to Simple Atoms*

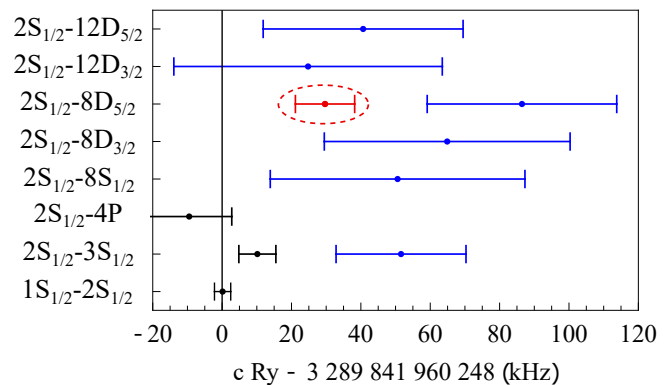


FIG. 5. A comparison of the Rydberg constant determined through Eqn 1 from one experimentally determined hydrogen interval. These determinations require a precise r_p value, which was taken from the muonic hydrogen measurement alone [14]. Blue points were measured in Paris (2S-3S [16], 2S-8S/D [26], 2S-12D [19]), black points were measured in Garching ($1S_{1/2}$ - $2S_{1/2}$ [32], $2S_{1/2}$ - $3S_{1/2}$ [10], $2S_{1/2}$ -4P [9]), and our result is circled in red. As described in the text, we have subtracted the $1S_{1/2}$ - $2S_{1/2}$ interval [32] from the $1S_{1/2}$ - $3S_{1/2}$ measurements [10, 16]

(Springer, 2007).

- [3] P. J. Mohr, D. B. Newell, B. N. Taylor, CODATA recommended values of the fundamental physical constants: 2014, *Rev. Mod. Phys.* **88**, 1 (2016).
 [4] S. G. Karshenboim, V. G. Ivanov, Hyperfine structure of the ground and first excited states in light hydrogen-like atoms and high-precision tests of QED, *Eur. Phys. J. D* **19**, 13 (2002).
 [5] M. S. Safronova, D. Budker, D. Demille, D. F. Kimball, A. Derevianko, C. W. Clark, Search for new physics with atoms and molecules, *Rev. Mod. Phys.* **90**, 025008 (2018).
 [6] L. C. Tu, J. Luo, Experimental tests of Coulomb's Law and the photon rest mass, *Metrologia* **41**, 136 (2004).
 [7] S. G. Karshenboim, Precision physics of simple atoms and constraints on a light boson with ultraweak coupling, *Phys. Rev. Lett.* **104**, 40801 (2010).
 [8] M. P. A. Jones, R. M. Potvliege, M. Spannowsky, Probing new physics using Rydberg states of atomic hydrogen, *Phys. Rev. Res.* **2**, 013244 (2020).
 [9] A. Beyer, L. Maisenbacher, A. Matveev, R. Pohl, K. Khabarova, A. Grinin, T. Lamour, D. C. Yost, T. W. Hänsch, N. Kolachevsky, T. Udem, The Rydberg constant and proton size from atomic hydrogen, *Science* **358**, 79 (2017).
 [10] A. Grinin, A. Matveev, D. C. Yost, L. Maisenbacher, V. Wirthl, R. Pohl, T. W. Hänsch, T. Udem, Two-photon frequency comb spectroscopy of atomic hydrogen, *Science* **370**, 1061 (2020).
 [11] M. Horbatsch, E. A. Hessels, Tabulation of the bound-state energies of atomic hydrogen, *Phys. Rev. A* **93**, 022513 (2016).
 [12] R. Pohl, A. Antognini, F. Nez, F. D. Amaro, F. Biraben, J. M. R. Cardoso, D. S. Covita, A. Dax, S. Dhawan, L. M. P. Fernandes, A. Giesen, T. Graf, T. W. Hänsch, P. Indelicato, L. Julien, C. Y. Kao, P. Knowles, E. O. Le Bigot, Y. W. Liu, J. A. M. Lopes, L. Ludhova, C. M. B. Monteiro, F. Mulhauser, T. Nebel, P. Rabi-

- nowitz, J. M. F. Dos Santos, L. A. Schaller, K. Schuhmann, C. Schwob, D. Taquu, J. F. C. A. Veloso, F. Kottmann, The size of the proton, *Nature* **466**, 213 (2010).
- [13] A. Antognini, F. Nez, K. Schuhmann, F. D. Amaro, F. Biraben, J. M. R. Cardoso, D. S. Covita, A. Dax, S. Dhawan, M. Diepold, L. M. P. Fernandes, A. Giesen, A. L. Gouvea, T. Graf, T. W. Hänsch, P. Indelicato, L. Julien, C. Y. Kao, P. Knowles, F. Kottmann, E. O. Le Bigot, Y. W. Liu, J. A. M. Lopes, L. Ludhova, C. M. B. Monteiro, F. Mulhauser, T. Nebel, P. Rabinowitz, J. M. F. Dos Santos, L. A. Schaller, C. Schwob, D. Taquu, J. F. C. A. Veloso, J. Vogelsang, R. Pohl, Proton structure from the measurement of 2S-2P transition frequencies of muonic hydrogen, *Science* **339**, 417 (2013).
- [14] R. Pohl, R. Gilman, G. A. Miller, K. Pachucki, Muonic hydrogen and the proton radius puzzle, *Annu. Rev. Nucl. Part. Sci.* **63**, 175 (2013).
- [15] C. E. Carlson, The proton radius puzzle, *Prog. Part. Nucl. Phys.* **82**, 59 (2015).
- [16] H. Fleurbaey, S. Galtier, S. Thomas, M. Bonnaud, L. Julien, F. Biraben, F. Nez, M. Abgrall, J. Guéna, New Measurement of the 1S-3S Transition Frequency of Hydrogen: Contribution to the Proton Charge Radius Puzzle, *Phys. Rev. Lett.* **120**, 183001 (2018).
- [17] N. Bezginov, T. Valdez, M. Horbatsch, A. Marsman, A. C. Vutha, E. A. Hessels, A measurement of the atomic hydrogen Lamb shift and the proton charge radius, *Science* **365**, 1007 (2019).
- [18] F. Biraben, J. C. Garreau, L. Julien, Détermination of the rydberg constant by doppler-free two-photon spectroscopy of hydrogen rydberg states, *Epl* **2**, 925 (1986).
- [19] B. De Beauvoir, C. Schwob, O. Acef, L. Jozefowski, L. Hilico, F. Nez, L. Julien, A. Clairon, F. Biraben, Metrology of the hydrogen and deuterium atoms: Determination of the Rydberg constant and Lamb shifts, *Eur. Phys. J. D* **12**, 61 (2000).
- [20] S. F. Cooper, A. D. Brandt, C. Rasor, Z. Burkley, D. C. Yost, Cryogenic atomic hydrogen beam apparatus with velocity characterization, *Rev. Sci. Instrum.* **91**, 013201 (2020).
- [21] Z. Burkley, A. D. Brandt, C. Rasor, S. F. Cooper, D. C. Yost, Highly coherent, watt-level deep-UV radiation via a frequency-quadrupled Yb-fiber laser system, *Appl. Opt.* **58**, 1657 (2019).
- [22] S. F. Cooper, Z. Burkley, A. D. Brandt, C. Rasor, D. C. Yost, Cavity-enhanced deep ultraviolet laser for two-photon cooling of atomic hydrogen, *Opt. Lett.* **43**, 1375 (2018).
- [23] M. A. Lombardi, The Use of GPS Disciplined Oscillators as Primary Frequency Standards for Calibration and Metrology Laboratories, *NCSLI Meas.* **3**, 56 (2008).
- [24] T. Udem, L. Maisenbacher, A. Matveev, V. Andreev, A. Grinin, A. Beyer, N. Kolachevsky, R. Pohl, D. C. Yost, T. W. Hänsch, Quantum Interference Line Shifts of Broad Dipole-Allowed Transitions, *Ann. Phys.* **531**, 1900044 (2019).
- [25] C. Schwob, L. Jozefowski, B. De Beauvoir, L. Hilico, F. Nez, L. Julien, F. Biraben, O. Acef, A. Clairon, Optical frequency measurement of the 2S-12D transitions in hydrogen and deuterium: Rydberg constant and lamb shift determinations, *Phys. Rev. Lett.* **82**, 4960 (1999).
- [26] B. De Beauvoir, F. Nez, L. Julien, B. Cagnac, F. Biraben, D. Touahri, L. Hilico, O. Acef, A. Clairon, J. J. Zondy, Absolute frequency measurement of the 2S-8S/D transitions in hydrogen and deuterium: New determination of the rydberg constant, *Phys. Rev. Lett.* **78**, 440 (1997).
- [27] M. Haas, U. D. Jentschura, C. H. Keitel, N. Kolachevsky, M. Herrmann, P. Fendel, M. Fischer, T. Udem, R. Holzwarth, T. W. Hänsch, M. O. Scully, G. S. Agarwal, Two-photon excitation dynamics in bound two-body Coulomb systems including ac Stark shift and ionization, *Phys. Rev. A - At. Mol. Opt. Phys.* **73**, 052501 (2006).
- [28] A. E. Kramida, A critical compilation of experimental data on spectral lines and energy levels of hydrogen, deuterium, and tritium, *At. Data Nucl. Data Tables* **96**, 586 (2010).
- [29] B. H. Porter, Research applications of colloidal graphite, *Rev. Sci. Instrum.* **7**, 101 (1936).
- [30] I. I. Sobel'man, L. A. Vainshtein, A. Y. Evgenii, *Excitation of Atoms and Broadening of Spectral Lines* (Springer-Verlag Berlin Heidelberg New York, 1955).
- [31] A. Matveev, N. Kolachevsky, C. M. Adhikari, U. D. Jentschura, Pressure shifts in high-precision hydrogen spectroscopy: II. Impact approximation and Monte-Carlo simulations, *J. Phys. B At. Mol. Opt. Phys.* **52**, 75006 (2019).
- [32] C. G. Parthey, A. Matveev, J. Alnis, B. Bernhardt, A. Beyer, R. Holzwarth, A. Maistrou, R. Pohl, K. Predehl, T. Udem, T. Wilken, N. Kolachevsky, M. Abgrall, D. Rovera, C. Salomon, P. Laurent, T. W. Hänsch, Improved Measurement of the Hydrogen 1S-2S Transition Frequency, *Phys. Rev. Lett.* **107**, 203001 (2011).
- [33] E. Tiesinga, P. J. Mohr, D. B. Newell, B. N. Taylor, Codata recommended values of the fundamental physical constants: 2018, *Rev. Mod. Phys.* **93**, 25010 (2021).

Supplement for:

Measurement of the $2S_{1/2}$ - $8D_{5/2}$ transition in hydrogen

A. D. Brandt, S. F. Cooper, C. Rasor, Z. Burkley,* and D. C. Yost[†]

Department of Physics, Colorado State University, Fort Collins, CO 80523

A. Matveev

Russian Quantum Center, Skolkovo, Moscow 143025, Russia

(Dated: November 19, 2021)

I. DATA ANALYSIS

A. Lineshape fitting function

In recent laser spectroscopy of hydrogen, experimentally obtained resonances have been fit with physically-motivated analytic functions [24, 25], or numeric lineshape models [21]. In this measurement, we have chosen the former.

To obtain these analytic functions, we begin with the optical Bloch equations. For the 2S-8D transition, the 8D atoms preferentially decay back to the 1S state through nP states, with only about 5% decaying back to the 2S state [4]. If we assume that the population in the upper state is small and that the coherences adiabatically follow the populations, the optical Bloch equations may be approximated as

$$\dot{\rho}_{gg} = -\Omega \text{Im}(\rho_{ge}) \quad (1)$$

$$0 = -i 2\pi \Delta\nu \rho_{ge} + i \frac{\Omega}{2} \rho_{gg} - \frac{\gamma}{2} \rho_{ge} \quad (2)$$

$$0 = \Omega \text{Im}(\rho_{ge}) - \gamma \rho_{ee}, \quad (3)$$

where Ω is the two-photon Rabi frequency, γ is the decay rate from the excited state, and $\Delta\nu$ is the detuning from the two-photon resonance. Since we are detecting the population remaining in the ground state, we decouple the differential equations to find

$$\dot{\rho}_{gg} = -\frac{1}{4} \frac{\gamma \Omega^2}{(2\pi \Delta\nu)^2 + (\gamma/2)^2} \rho_{gg}. \quad (4)$$

The solution, assuming a time-dependent Rabi frequency, is given by

$$\rho_{gg}(t) = \exp\left(-\frac{1}{4} \frac{\gamma \int_0^t \Omega^2 d\tau}{(2\pi \Delta\nu)^2 + (\gamma/2)^2}\right). \quad (5)$$

Here, we have assumed that the detuning is constant, which is only approximately true due to the varying AC Stark shift as the atom traverses the laser beam. From Eqn. 5, we find that a physically motivated fit function is given by

$$\mathcal{F}(A, \alpha, \nu_0, \gamma_0) = A \exp[-\mathcal{L}_0(\alpha, \nu_0, \gamma_0)], \quad (6)$$

where \mathcal{L}_0 is a Lorentzian function with width γ_0 , ν_0 is the center frequency of the transition, α is the Lorentzian amplitude, and A accounts for the off-resonant metastable count rate.

* Now at Dep. Physik, ETH Zürich

† Dylan.Yost@colostate.edu

The $2S_{1/2}-8D_{5/2}$ transition also contains unresolved hyperfine structure that must be taken into account ($F=2$ and $F=3$). To account for this structure, we adjust our fitting function to give

$$\mathcal{F}(A, \alpha_2, \alpha_3, \nu_2, \nu_3, \gamma_2, \gamma_3) = A \exp[-\mathcal{L}_0(\alpha_2, \nu_2, \gamma_2) - \mathcal{L}_0(\alpha_3, \nu_3, \gamma_3)], \quad (7)$$

where the subscript denotes the hyperfine component of the $8D_{5/2}$ level. The ratio of α_2 and α_3 is given by $\alpha_3/\alpha_2 = 3.5$ due to the relative strengths of the transitions – this is independent of laser polarization. In addition, the natural linewidth and transit-time broadening are both independent of the hyperfine state so that we can safely assume that $\gamma_2 = \gamma_3$. Finally, the hyperfine splitting of the $8D_{5/2}$ state is known and given by $\text{HFS} = 142.43$ kHz [5] which gives a fixed relationship between ν_3 and ν_2 – in practice we use the detuning from the centroid frequency, ν_c , as the fit parameter. Therefore, we fit our experimental lines with

$$\mathcal{F}(A, \alpha, \nu_c, \gamma) = A \exp[-\alpha(\mathcal{L}_2(\nu_c, \gamma) + \mathcal{L}_3(\nu_c, \gamma))], \quad (8)$$

where the ratio of the amplitudes of the Lorentzian functions (\mathcal{L}_2 and \mathcal{L}_3) are in a fixed ratio of 1 to 3.5. An example of a single scan fit with Eqn. 8 is shown in supplemental Fig. 1.

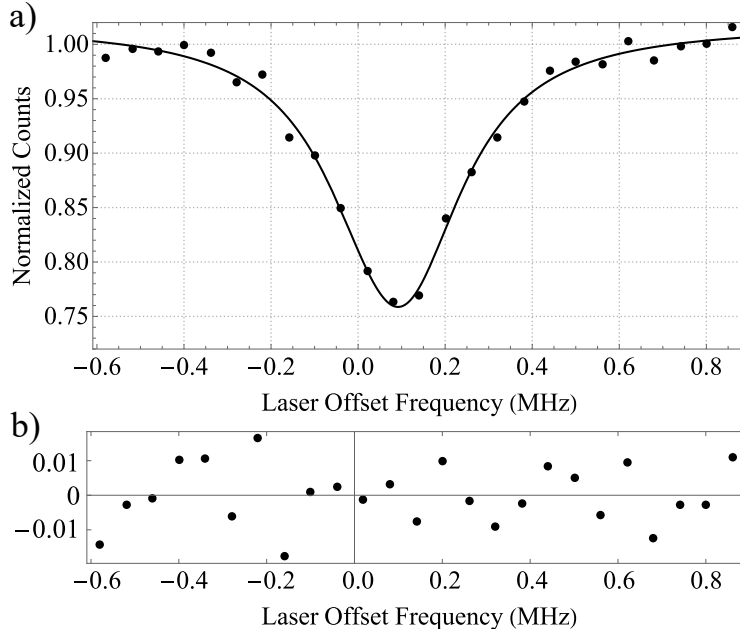


FIG. 1. A single scan of the $2S_{1/2}-8D_{5/2}$ line fit with Eq. 8. The off-resonant count rate normalized to unity. A typical off-resonant count rate is $\approx 10^4$ /s. a) A single scan fit and b) a single scan fit residuals. A shot noise limited signal-to-noise ratio of $\approx 10^2$ is expected for the given count rates.

B. The AC Stark shift extrapolations

To account for the AC Stark shift, we perform scans of the resonance at various laser powers, determine the centroid frequencies for individual scans, and extrapolate these to zero laser power. For these extrapolations, we again use simple, analytic functions, which we justify below.

The shift due to the AC Stark effect can be written as

$$\Delta\nu_{ac} = \beta_{ac}I(t) \quad (9)$$

where β_{ac} is the AC Stark coefficient [6]. While the AC Stark shift is itself linear, the extrapolations can exhibit nonlinear behavior when measuring ensembles of trajectories and when appreciable saturation of the transition occurs. In the case of many atomic trajectories contributing to the overall line, the contribution of each trajectory is weighted by the population driven in that particular trajectory. Therefore, the average AC Stark shift is

$$\langle \Delta\nu_{ac} \rangle = \frac{\int \mathcal{D}(s) (1 - \rho_{gg}(s)) \Delta\nu_{ac}(s) ds}{\int \mathcal{D}(s) (1 - \rho_{gg}(s)) ds}, \quad (10)$$

where $\mathcal{D}(s)$ represents the spatial distribution of atomic trajectories, and s is the transverse distance from the peak of the 778 nm Gaussian intensity profile. The spectroscopy signal is determined by counting the quenched fraction of the metastable atoms, given by $1 - \rho_{gg}(s)$. From the analysis of the $2S_{1/2}$ - $8D_{5/2}$ lineshapes above, we find a functional form for the spectroscopy signal given by

$$1 - \rho_{gg}(s) = 1 - \exp[-\kappa P_0^2 e^{-ks^2}], \quad (11)$$

where κ and k are scaling constants, and P_0 is laser power within the optical cavity. This follows from Eq. (5) and the fact that Ω is proportional to P_0 for two-photon transitions [6]. For low intracavity power, $\rho_{gg}(s) \approx 1 - \kappa e^{-ks^2} P_0^2$ and

$$\langle \Delta\nu_{ac} \rangle = \frac{\int \mathcal{D}(s) e^{-ks^2} P_0^2 (P_0 \beta_{ac} e^{-ks^2}) ds}{\int \mathcal{D}(s) e^{-ks^2} P_0^2 ds} = P_0 \frac{\int f(s) ds}{\int g(s) ds}, \quad (12)$$

where $f(s)$ and $g(s)$ are spatially dependent functions without P_0 dependence. From this we see that $\Delta\nu_{ac}$ is proportional to the intracavity laser power and a linear extrapolation is suitable.

We may estimate the effect of saturation by keeping an additional term in the series expansion of $1 - \rho_{gg}(s)$. In that case, $(1 - \rho_{gg}(s)) \approx \kappa e^{-ks^2} P_0^2 - \frac{1}{2} \kappa^2 e^{-2ks^2} P_0^4$. Substituting this approximation of $1 - \rho_{gg}$, we find

$$\langle \Delta\nu_{ac} \rangle \approx h_1 P_0 - h_2 P_0^3, \quad (13)$$

where h_1 and h_2 are constants determined by the spread of metastable atomic trajectories and the width of the spectroscopy laser beam's transverse Gaussian profile. Therefore, the nonlinearity introduced to the AC extrapolation is predominantly cubic. One should note that this conclusion does not rely on the exact form of the metastable distribution, $\mathcal{D}(s)$, and the accuracy of this result has been confirmed with the numeric model (described in the next section).

C. Numeric Model

The numeric model is used primarily for quantifying the DC Stark shifts and to verify that fitting functions described above are sufficiently accurate. We have developed a numeric model based on density matrices, which allows for a description of repopulation of the 2S state, and a model based on state amplitudes. We have found that the repopulation of the 2S state via spontaneous emission produces shifts of $< \pm 10$ Hz in the extrapolated AC-Stark-shift-free resonance frequency. Therefore, we focus on the state amplitude treatment here, since that treatment allows for the inclusion of DC Stark effects in a much simpler manner.

Roughly 15 cm before the spectroscopic region, the 2S state is populated via a two-photon excitation with 243 nm laser radiation tuned to the $1S_{1/2}^{F=1}$ to $2S_{1/2}^{F=1}$ transition. The hyperfine splitting of the 1S and 2S states is large enough that there is effectively no population in the $2S^{F=0}$ state. We assume that our ground state (1S) atoms are equally populated in the $F = 1$, $m_F = 0, \pm 1$ levels. Since, the $1S_{m_F=\pm 1}^{F=1} \rightarrow 2S_{m_F=\pm 1}^{F=1}$ and $1S_{m_F=0}^{F=1} \rightarrow 2S_{m_F=0}^{F=1}$ matrix elements have the same magnitude [6], the 2S $F = 1$ hyperfine manifold is equally populated as well. The lifetime of the $2S_{1/2}$ state is ≈ 122 ms so no appreciable decay occurs in the ≈ 1 ms transit time of the metastable beam through the apparatus. We choose to drive the $2S_{1/2}$ - $8D_{5/2}$ transition with linearly polarized light, which defines the z -axis in the experiment. The two-photon selection rules for $\Delta L = 2$ using linearly polarized light, and with the laser polarization defining quantization axis, dictate that $\Delta m_F = 0$ [6].

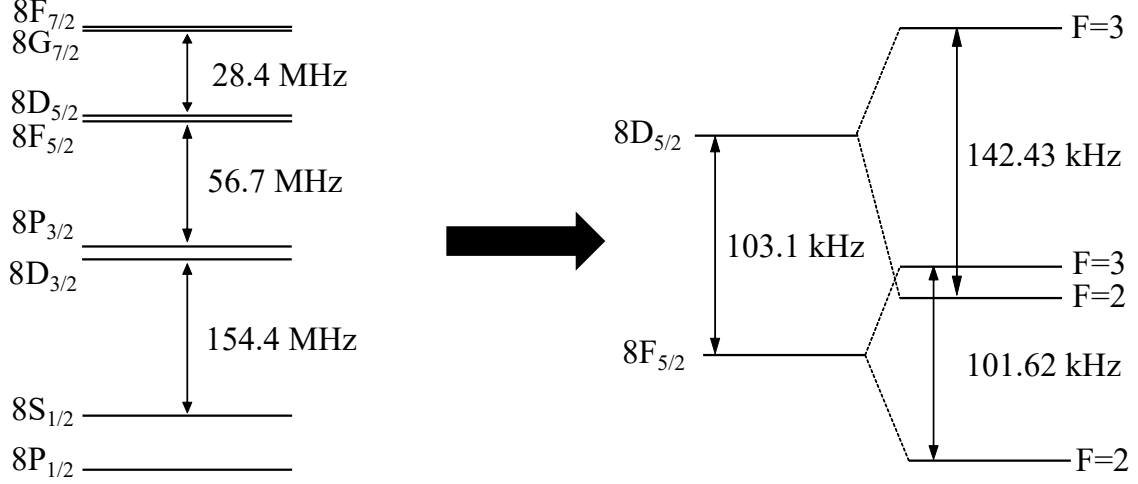


FIG. 2. Level structure of the relevant states in the $n = 8$ manifold.

The couplings introduced by the DC electric field causes a quadratic shift due to nearby dipole-allowed transitions and a lineshape distortion due to the mixing of the nearly degenerate $8D_{5/2}$ and $8F_{5/2}$ states [4]. The quadratic shift due to nearby dipole-allowed transitions is calculated with second-order perturbation theory. Both the mixing and the quadratic shift are included in the state amplitude equations.

We label the state amplitudes for the hyperfine components of the $2S_{1/2}$, $8D_{5/2}$, and $8F_{5/2}$ levels with g , e , and f respectively. The coupled set of differential equations describing the interaction is given by

$$\dot{c}_g = -i \sum_e \frac{\Omega_{ge}}{2} c_e, \quad (14)$$

$$\dot{c}_e = (i\Delta\omega_e - \frac{\gamma_e}{2})c_e - i\frac{\Omega_{ge}}{2}c_g - \frac{i}{\hbar} \sum_f U_{ef}c_f, \quad (15)$$

$$\dot{c}_f = (i\Delta\omega_f - \frac{\gamma_f}{2})c_f - \frac{i}{\hbar} \sum_e U_{fe}c_e, \quad (16)$$

$$\Delta\omega_e = 2\omega - (\omega_{ge} + \delta\omega_{\mathcal{E}}^{(e)} \mathcal{E}^2 + \delta_{ge}(t)), \quad (17)$$

$$\Delta\omega_f = 2\omega - (\omega_{gf} + \delta\omega_{\mathcal{E}}^{(f)} \mathcal{E}^2 + \delta_{gf}(t)), \quad (18)$$

where ω is the laser frequency, $\omega_{ij} = \omega_j - \omega_i$ is the resonance frequency separating states $|i\rangle$ and $|j\rangle$, \mathcal{E} is the magnitude of the stray electric field, Ω_{ij} is the trajectory-dependent Rabi frequency [6], $\delta\omega_{\mathcal{E}}^{(i)}$ is the quadratic Stark shift coefficient for state $|i\rangle$, δ_{ij} is the combined AC Stark and second order-Doppler detuning terms, and U_{ij} is the perturbing matrix element connecting states $|i\rangle$ and $|j\rangle$ (i.e. $-\langle i|\vec{\mathcal{E}} \cdot q\vec{r}|j\rangle$). The combined detuning of the AC Stark effect and the second-order Doppler effect is given by

$$\delta_{ij} = 2\pi[\beta_{ac}(j) - \beta_{ac}(i)]I(t, v, s) - \frac{v^2}{2c^2}\omega_{ij}, \quad (19)$$

where $\beta_{ac}(j)$ is the state dependent AC Stark shift coefficient. $I(t, v, s)$ is the time-dependent intensity seen by an atom traversing through the laser beam a distance s away from the Gaussian beam center at velocity v , which is given by

$$I(t, v, s) = I_0 \text{Exp} \left(-2 \frac{v^2 t^2 \sin^2(\theta)}{w^2} - 2 \frac{s^2}{w^2} \right). \quad (20)$$

The time-dependent Rabi frequency seen by an atom in a specific trajectory is likewise given by

$$\Omega_{ij}(t) = 2(2\pi\beta_{ij})I(t, v, s), \quad (21)$$

where β_{ij} is the two-photon matrix element connecting states $|i\rangle$ and $|j\rangle$ [6]. For each trajectory, we numerically integrate Eqns. (14-16) to find a lineshape $\tilde{L}(\omega, s, v)$. To include the effect of the different trajectories, we integrate $\tilde{L}(\omega, s, v)$ over a spatial and velocity distribution $\rho(s, v)$ to find the full linshape, given by

$$L(\omega) = \iint \tilde{L}(\omega, s, v) \rho(s, v) ds dv. \quad (22)$$

The function $\rho(s, v)$ is determined by time-of-flight measurements [7], and the geometric constraints set by the metastable hydrogen/243 nm light overlap and the divergence of the atomic hydrogen beam.

The distortion present on the $2S_{1/2}$ - $8D_{5/2}$ and the $2S_{1/2}$ - $12D_{5/2}$ lineshapes is used to quantify the magnitude of the electric field. A single scan of the $2S_{1/2}$ - $8D_{5/2}$ resonance is insufficient to quantify the distortion, therefore many scans are averaged together before being fit with the numeric model. When averaging lines, we choose several lines with nominally equal photodiode voltage. For averaging, we have chosen a PD voltage that corresponds to quenching approximately 20% of the total metastable flux. We find that the electric fields determined *in situ* on the $2S_{1/2}$ - $8D_{5/2}$ lines are consistent with the determinations of the

electric field on the $2S_{1/2}$ - $12D_{5/2}$ lines. Examples of the $2S_{1/2}$ - $8D_{5/2}$ and $2S_{1/2}$ - $12D_{5/2}$ lines fit with the numeric model are shown in supplemental Fig. 3.

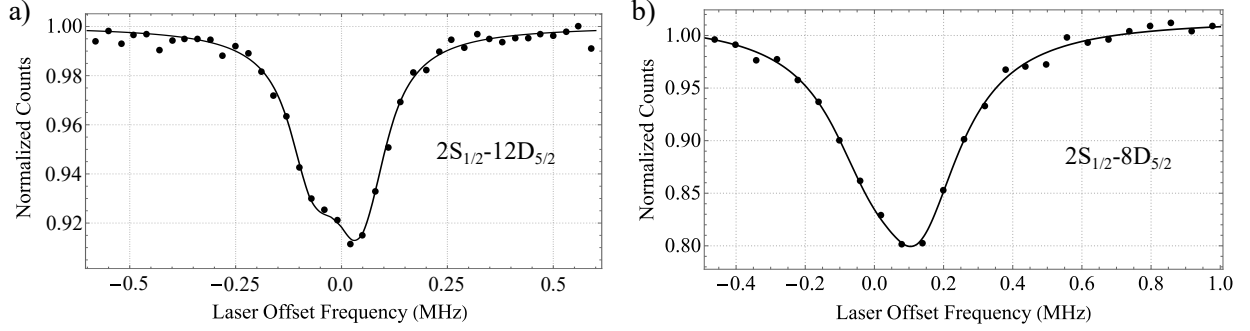


FIG. 3. Electric field characterization. a) Example of measured $2S_{1/2} - 12D_{5/2}$ lineshape fit with the numeric model. This corresponds to a field strength of 3 mV/cm b) Example of measured $2S_{1/2} - 8D_{5/2}$ lineshape, composed of 27 scans averaged together fit with the numeric model. This line fit corresponds to a 6.5 mV/cm field, which is the largest field present in the data.

We find that the distortion present on the experimentally measured $2S_{1/2}$ - $12D_{5/2}$ lineshapes is insensitive to the polarization of the spectroscopy light. However, from investigations with the lineshape model, we find that the nature of the distortion is highly contingent upon the relative orientation of the stray field and the spectroscopy light. From this, we conclude that the stray electric field must be nearly perpendicular to all possible laser polarizations – i.e. along the direction of the light propagation. In Fig. 4, we show the $2S_{1/2}$ - $12D_{5/2}$ line excited by four linear polarizations (horizontal, vertical, $\pm 45^\circ$) on a given day with the same lineshape generated by the numeric model overlaid. As shown in the figure, the distortion is consistent as the polarization is rotated. We have additionally included an example of the $2S_{1/2}$ - $12D_{5/2}$ modeled lineshape under the influence of a uniform electric field as the relative orientation of the light polarization and stray field is varied, which shows a clear variation in the lineshape as the relative angle changes. We have investigated this polarization dependence of the $2S_{1/2}$ - $12D_{5/2}$ line after multiple batches of data acquisition and have found similar insensitivity to the light polarization, indicating that the stray field orientation was nearly perpendicular to the light field throughout the experiment.

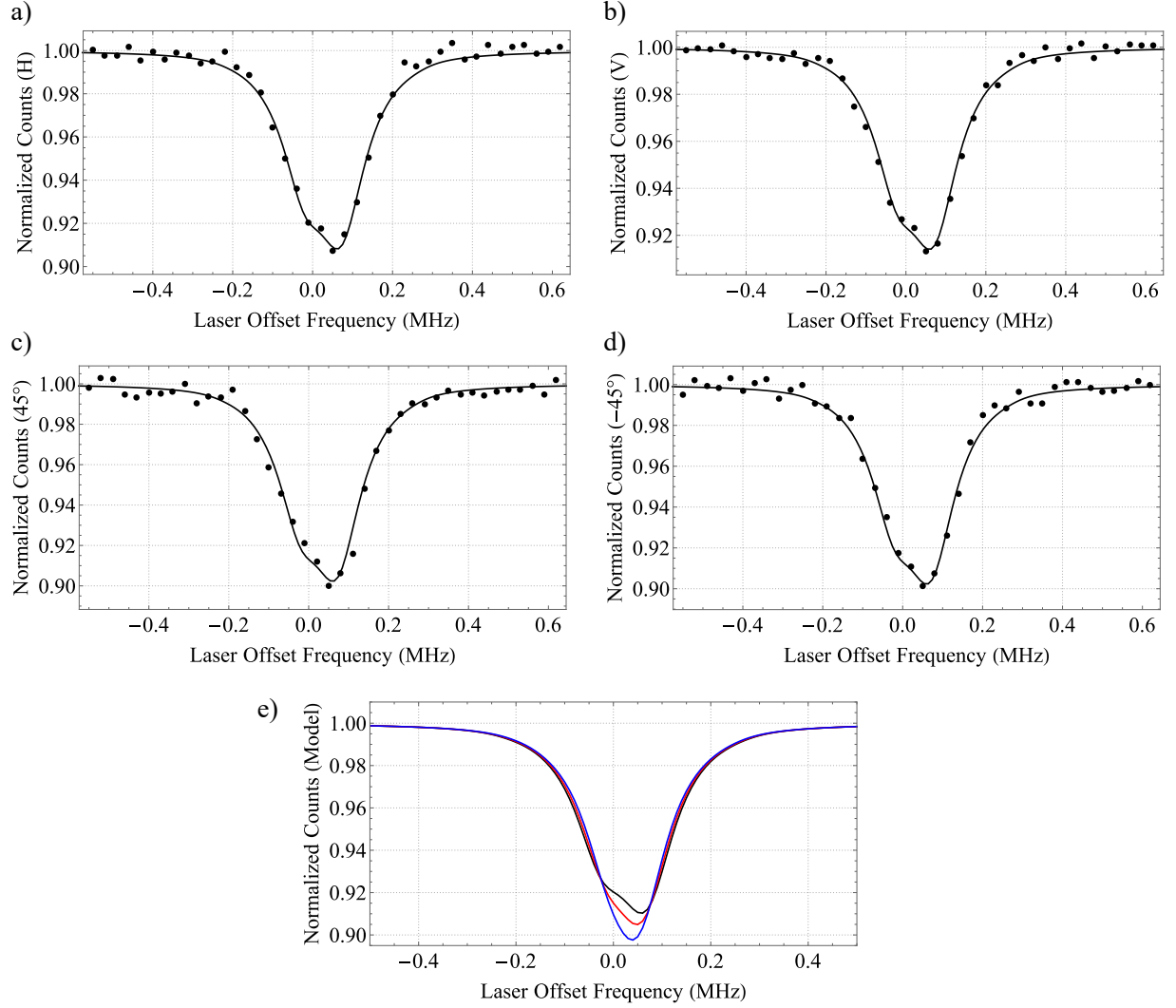


FIG. 4. Example $2S_{1/2}$ - $12D_{5/2}$ lineshapes excited by distinct linear polarizations. We overlay the data with simulated data for a stray field of 2.5 mV/cm perpendicular to the polarization of the light field. Each lineshape is composed of ≈ 30 averaged scans. a) Horizontal polarization. b) Vertical polarization. c) 45° . d) -45° . e) Numerically modeled $2S_{1/2}$ - $12D_{5/2}$ lines under the influence of a uniform field of 2.5 mV/cm. The relative angle between the light polarization and stray field is 90° (black), 55° (red), and 35° (blue).

D. Statistics

Before fitting each scan of the $2S_{1/2}$ - $8D_{5/2}$ resonance with the fit function, $\mathcal{F}(A, \alpha, \nu_c, \gamma)$, we first remove data points where there was a problem with excitation of the $1S$ - $2S$ transition due to laser lock breaks, which manifest as far statistical outliers in the metastable count

rate. Similarly, spurious lock breaks of the 778 nm power enhancement cavity are removed, which are evident on the 778 nm transmission diode. A scan of the $2S_{1/2}-8D_{5/2}$ resonance is composed of 25 frequency points if no outliers are removed – scans composed of fewer than 20 points are omitted entirely from the data analysis. In a typical day of data acquisition, less than 5% of all individual data points are omitted. When fitting scans with $\mathcal{F}(A, \alpha, \nu_c, \gamma)$, each data point in the scan is weighted by the estimated shot noise for that point.

The reduced chi-squared statistic is used to quantify to goodness-of-fit when analyzing individual resonance scans. We first assign error bars to the individual data points based on shot noise. This results in a $\chi_k^2 \approx 1.5$ on average. Here, k denotes the degrees of freedom, which is typically 21 for a full scan of 25 points with 4 fit parameters. While χ_k^2 is typically greater than one, this is expected due to the contribution of some technical noise arising from variations in the atomic beam flux. Therefore, the error bars on the individual data points are scaled until $\chi_k^2 = 1$ for a given scan – fluctuation of the metastable flux is not associated with any shift (possible density effects are discussed later and shown to be negligible).

Each line fit results in a hyperfine centroid ($\nu_c \pm \sigma_c$) for a given 778 nm photodiode voltage V , which is proportional to the intracavity power. In a day of data acquisition, the set of $\{V^{(i)}, \nu_c^{(i)}\}$ obtained from the scans of the resonance allow for an AC Stark extrapolation to zero intracavity power. The data set is fit with a cubic function of the form $\nu_c(V) = \nu_0 + aV + bV^3$, with each ordered pair in the data set weighted by the associated $1/\sigma_c^2$ for that data point. For these fits, we typically find $\chi_N^2 \approx 0.95$ for a given day. Since χ_N^2 itself has a variance of $\sqrt{2/N}$, this is reasonable (a typical extrapolation has $N \approx 200$). For a given day’s worth of data, we then correct the extrapolated centroid frequency for the DC Stark shift (see main text for further discussion).

We obtained 17 days’ worth of data (shown in the main text) and calculate the statistical mean of the resonance frequency, $\bar{\nu}$, and variance, $\bar{\sigma}_\nu$, for the entire set. The variance of the mean frequency is given by $\bar{\sigma}_\nu = \left(\sqrt{\sum 1/\sigma_{\nu,i}^2}\right)^{-1} = 1.2$ kHz. The scatter within the full set is in excellent agreement with statistical fluctuations as we find a reduced chi-squared statistic of 1.05. Therefore, there is no evidence of significant and varying systematic effects in the data set.

II. MINOR SYSTEMATIC CORRECTIONS

Our method for accounting for our two largest systematic effects, the AC and DC Stark shifts, is addressed in the main text and the preceding sections. Here, we discuss smaller systematic effects.

A. Second-order Doppler shift

The second-order Doppler effect enters as $\Delta\nu_{DS} = -\frac{1}{2}(v/c)^2\nu$, where v is the atom velocity in the lab frame, c is the speed of light, and ν is the rest-frame resonance frequency. We have characterized the velocity distribution of our metastable hydrogen beam through time-of-flight measurements [7]. From these investigations, we have found that the velocity distribution is modified from a Maxwell-Boltzmann distribution by the excitation and detection dynamics to $P(v) \propto v^4 e^{-\beta v^2}$, with $\beta = m/2k_b T$. The temperature of the atomic beam is estimated with a silicon diode temperature probe mounted on the surface of the cryogenic nozzle.

Investigations with the numeric lineshape model indicate that the net second-order Doppler shift on an ensemble of atoms is well-approximated by calculating the shift associated with the most-probable velocity class. The uncertainty associated with the most-probable velocity for a given nozzle temperature reading is < 10 m/s. Fitting the time-of-flight measurements obtained in [7] gives a second-order Doppler shift of $-1475(25)$ Hz at 9.5 K and $-930(11)$ Hz at 5.9 K. Spectroscopy was performed on the atomic beam for temperatures between 4.5 K and 4.9 K, which corresponds to a second-order Doppler shift of $-0.73(10)$ kHz. This shift is corrected for in our final measurement as indicated in the main text.

B. Zeeman effect

We passively mitigate Earth's magnetic field with a pair of concentric magnetic shields composed of high-permeability metal (mu-metal) centered around the 778 nm light/atom interaction region. We have simulated the attenuation of Earth's field in the center of the shields and we expect residual magnetic fields of less than 1 mG within the spectroscopic volume.

The linear Zeeman effect causes a shift of a magnetic sublevel with quantum number m_F , which is given by

$$\Delta E_Z/\hbar = -\langle \psi | \vec{\mu} \cdot \vec{B} | \psi \rangle = \frac{1}{\hbar} g_F \mu_B m_F B, \quad (23)$$

where B is the magnetic flux density, g_F is the g-factor, and μ_B is the Bohr magneton. With linearly polarized spectroscopy light the linear Zeeman effect only causes a broadening of the resonance. However, with circularly polarized light oriented about a stray magnetic field, a shift can occur.

In order to quantify the possibility of a residual Zeeman shift, we have also performed spectroscopy of the $2S_{1/2}$ - $8D_{5/2}$ transition with σ^+ and σ^- light of similar intensity. The splitting of these two lines amounts to maximum of 3.7 kHz (limited by the statistics of the measurement), indicating that the maximal possible Zeeman shift is 1.9 kHz. From the maximal possible shift of 1.9 kHz, we estimate a magnetic field strength of 0.6 mG, which is in good agreement with our magnetic shields simulation.

This maximal 1.9 kHz shift is suppressed by the polarization purity of the spectroscopy light. We have measured the polarization purity by determining the maximum polarization extinction ratio, given as R , with a polarizing beamsplitter after the 778 nm enhancement cavity and found that $R \leq 0.01$. This leads to a maximum imbalance in the right versus left components of $\approx 20\%$. By assuming this maximum imbalance in the transition amplitudes between all hyperfine components, we find that the measured 1.9 kHz shift should be suppressed by a factor of ≈ 3.4 , leading to a maximal shift of 0.56 kHz from the Zeeman effect.

Since this represents an upper bound, we apply no shift and assume ± 0.56 kHz as the full uncertainty. Higher-order Zeeman corrections are negligible at our current level of precision.

C. Frequency calibration and laser spectrum

A GPS-trained Rb-oscillator (Stanford Research systems FS740) provides our absolute frequency reference. This source is used to reference two frequency counters which redundantly monitor the frequency comb repetition rate. Our optical frequency comb is based on an erbium-fiber oscillator centered at 1550 nm. The comb offset frequency, f_0 , is stabilized and a comb mode near 1550 nm is stabilized indirectly to an ultra-stable cavity with the help of a transfer laser oscillator. By measuring the repetition rate and phase locking f_0 of

the comb, the absolute frequency of all comb teeth are determined. Since the Coherent-899 Ti:Sapphire and the 972 nm ECDL (quadrupled to 243 nm to excite the 1S-2S transition) are coherently phase-locked to the comb, we can determine the absolute frequency of those lasers from the RF beat note frequencies.

The RF beat notes with the optical frequency comb can be converted into absolute atomic frequencies via

$$\nu_{1S-2S} = 8(nf_r + f_0 + f_{\text{beat}}^{972}) \quad (24)$$

for the 972 nm laser system and

$$\nu_{2S-8D} = 2(mf_r + 2f_0 + f_{\text{beat}}^{778}) \quad (25)$$

for the 778 nm spectroscopy laser. The factor of two multiplying f_0 arises because we frequency double the frequency comb output before performing the beat note with the 778 nm light. The repetition rate of the frequency comb is determined by the frequency counters over 100 s gates, and a typical day's data amounts to 5000-20000 s of f_r counting.

In principle, an asymmetric spectral distribution of the spectroscopy laser could pull the 2S-8D resonance. The phase noise of the 778 nm light is strongly suppressed by phase-locking to the frequency comb. Nevertheless, we have quantified the phase noise distribution on the 778 nm light by investigating the beat note. By convolving the observed spectral density with our fit function, we estimate the laser noise amounts to a 5 Hz shift and 2 kHz of line broadening. Both are negligible effects.

As mentioned in the main text, we have verified the absolute frequency calibration of the GPS-disciplined FS740 by locally counting a 5 MHz signal provided by the NIST WWVB station in Fort Collins, Colorado for 17 hours. We have found a fractional frequency counter offset of $+5 \times 10^{-13}$, which is within the expected performance of GPS-disciplined Rb-oscillators [8]. A typical day's worth of data is composed of 10^4 s of data, which corresponds to a frequency stability of 3×10^{-13} obtained from the Allan variation the Rb-oscillator. We apply a -0.40(40) kHz correction associated with the measured fractional frequency offset, and assume the frequency instability of the Rb-oscillator and offsets are uncorrelated. We therefore assign a frequency calibration correction of -0.40(47) kHz.

D. Blackbody radiation

The blackbody radiation emitted by nearby thermal surfaces perturbs the hydrogen atoms. The off-resonant contribution of the blackbody radiation causes an additional AC Stark shift while the resonant contribution dominantly reduces the lifetime of the states of interest. Numeric calculations of the blackbody shift at 300 K on the 8D states indicate that a shift of 0.49 kHz is expected [9] – the 2S state is unperturbed at our level of precision. The previous measurement of the 2S-8D transitions measured the blackbody shift at 300 K to be 0.65(16) kHz by heating the magnetic shields surrounding the spectroscopic volumes by 30 K [4], which is in excellent agreement with the theoretical estimation of 0.49 kHz. We therefore apply a blackbody correction of $-0.49(16)$ kHz.

E. Pressure Systematics

The most likely gas species to participate in collisions with the spectroscopy atoms are water and atomic hydrogen. Collisions between a hydrogen atom and a water molecule results in the hydrogen atom experiencing a varying electric field due to the intrinsic dipole moment of the water molecule, which is about $0.72 e a_0$ [10]. In contrast, collisions between hydrogen atoms are dominated by the Van der Waals interactions. To estimate potential shifts associated with pressure, we use the impact approximation [11, 12].

The linewidths of the 2S-8D and 2S-12D transitions obtained in preliminary measurements and at poor vacuum were broader than predicted by up to tens of kHz, with the 12D more strongly effected than the 8D line. We believe this broadening was due to collisions with water molecules. In a collision with a water molecule, hydrogen atoms in the 8D state may be quenched to nearby 8P and 8F states from the varying electric field.

To quantify possible shifts associated with such collisions, we have employed Monte Carlo simulations of the collisions between hydrogen and water molecules. From these simulations, we find a 16 GHz/Torr broadening and a 3 MHz/Torr shift on the 8D line and 37 GHz/Torr broadening, 3 MHz/Torr shift on the 12D line. For pressures in the range of a 10^{-6} Torr, this corresponds to ~ 10 kHz of broadening, which roughly agrees with our observation of broadened lines when we attempted to measure lines with relatively poor vacuum. The associated pressure shift is many order of magnitude below the associated broadening – 1

kHz of broadening would correspond to a ~ 0.1 Hz shift. While we do not see evidence of this broadening on our data used in the AC extrapolations, it is difficult to exclude the possibility of 1 kHz broadening on a ≈ 600 kHz line, and therefore set an upper limit of pressure shifts due to water collisions at 0.1 Hz.

In principle, the Van der Waals interaction between hydrogen atoms may also induce shifts on the $2S_{1/2}$ - $8D_{5/2}$ line. The Van der Waals interaction energy is given as

$$H_V = \frac{e^2}{4\pi\epsilon_0} \frac{x_1x_2 + y_1y_2 - 2z_1z_2}{R^3}, \quad (26)$$

which results in an associated energy shift of

$$\Delta E_V(n) = \sum_{m, m \neq n} \frac{|\langle n | H_V | m \rangle|^2}{E_n - E_m} = \frac{C_6}{R^6}, \quad (27)$$

with $|n\rangle = |n_1\rangle \otimes |n_2\rangle$ and $|m\rangle = |m_1\rangle \otimes |m_2\rangle$ being product states of atom 1 and atom 2. Here, we assume atom 1 to be the perturbing atom and atom 2 to be the perturbed atom. Under the impact approximation, the C_6 coefficient can be used to estimate the frequency shift due to Van der Waals interactions, which is given by

$$\Delta\omega_V \approx 2.9 \left(\frac{C_6}{\hbar} \right)^{2/5} v^{3/5} \mathcal{N}_p. \quad (28)$$

Here, v is the relative velocity between the two hydrogen atoms and \mathcal{N}_p is the number density [13, 24].

The Van der Waals interaction energy may be estimated with

$$\Delta E_V \sim \frac{1}{4\pi\epsilon_0 R^6} \mathcal{F}_{m_1, m_2} \frac{|\langle n_1, n_2 | r_1 r_2 | m_1, m_2 \rangle|^2}{E_{n_1} + E_{n_2} - E_{m_1} - E_{m_2}}, \quad (29)$$

where the integral-sum symbol indicates that the continuum contribution is also considered. For clarity, we have not included the angular factors seen in Eqn. 26, which is justified since we will find the possible systematic shifts associated with these collisions are very small. We make the substitution $\Delta(m_1) = E_{n_1} - E_{m_1}$, and rearrange the expression slightly to give

$$\Delta E_V \sim \frac{1}{4\pi\epsilon_0 R^6} \mathcal{F}_{m_1} |\langle n_1 | r_1 | m_1 \rangle|^2 \mathcal{F}_{m_2} \frac{|\langle n_2 | r_2 | m_2 \rangle|^2}{E_{n_1} + E_{n_2} + \Delta(m_1)}. \quad (30)$$

The sum (including the continuum contribution) over m_2 has a complicated closed form expression as a function of the energy difference $\Delta(m_1)$, which we will notate as $S(\Delta(m_1))$ – for this, we used the Sturmian formalism which may also be used to calculate the matrix elements and AC Stark coefficients for two-photon transitions [6, 14]. Therefore, calculating

the C_6 coefficients requires summing the squared dipole moments multiplied by $S(\Delta(m_1))$ over m_1 . While the sum over the bound states is straightforward, the continuum contribution is more difficult. As an upper bound for the continuum contribution, we multiply the maximal value of $S(\Delta(m_1))$ in the continuum by the total continuum contribution of the perturbing atom; the continuum contribution for the perturbing $|1S\rangle$ and $|2S\rangle$ hydrogen atoms can be found in [15] section 63, table 13 as $0.849 a_0^2$ and $2.7 a_0^2$ respectively. Additional care must be taken when the perturbing atom is in the $|2S\rangle$ state due to the near degeneracy of the 2S-8P and 2P-8D transitions. For these transitions, we assume the smallest energy splittings between the fine-structure components (≈ 1 GHz), and the largest dipole matrix element to provide the upper bound. From this, we find

$$C_6^{1S} \approx 5 \times 10^4 hc R_\infty a_0^6, \quad (31)$$

and

$$C_6^{2S} \approx 3 \times 10^{11} hc R_\infty a_0^6 \quad (32)$$

with the C_6^{2S} coefficient dominated by the near-degenerate contributions. We estimate an atomic hydrogen density of $10^{13}/\text{m}^3$ in our spectroscopic volume, with about 1% of those atoms in the metastable state. From Eqn. (28), this corresponds to a shift of ~ 1 Hz from Van der Waals interactions, which is far below our current level of precision.

F. Cross-damping

Of particular interest in many of the recent hydrogen measurements is an effect known as cross-damping, or quantum interference [16–19, 24, 25]. This effect appears when there are nearby off-resonant transitions and the fluorescence from spontaneous emission of the excited state is detected. This effect is almost entirely absent if all possible decay channels are equally accounted for, or if the remaining metastable population is detected instead of fluorescence [17, 19]. Since we are detecting remaining metastable population, our measurement is insensitive to this systematic.

G. $8D_{5/2}$ hyperfine structure

The hyperfine structure of the $8D_{5/2}$ state is unresolved and is therefore included into the lineshape fitting function. The splitting of the $F = 3$ and $F = 2$ manifolds of the $8D_{5/2}$

state is calculated to be 142.43(14) kHz [5]. Modifying the hyperfine splitting terms in the lineshape fitting function by ± 140 Hz results in shifts of the fit resonance frequency of ± 30 Hz, which we take as the uncertainty.

H. Photodiode Imperfections

The photodiode and data acquisition electronics recording the 778 nm cavity transmission has a small voltage offset of about < 5 mV that can vary slightly from day to day. This offset shifts the zero-intensity resonance frequency determined by the AC extrapolations. The AC Stark shift is about 300 kHz for a transmission PD voltage of 6 V. Therefore, the uncertainty introduced by a variation of 5 mV is about 250 Hz, which is taken as an additional uncertainty. Aside from DC offsets, a nonlinear response in the experimental detector would also introduce a shift to the AC extrapolated frequencies. Therefore, we have also tested the linearity of the experimental detector by comparing with a test detector. The 778 nm power is sent to the experimental detector, with a fraction of the light power picked off for the test detector. This data is then fit with the function

$$V_{exp} = a_V V_{test} + b_V V_{test}^2, \quad (33)$$

where a_V and b_V are fitting parameters. The ratio b_V/a_V sets the relative strength of the nonlinear response of the photodiode, and we find an upper bound of $b_V/a_V \approx 5 \times 10^{-4} V^{-1}$. This nonlinearity can be accounted for by adjusting the AC extrapolation fitting function to $\nu_c(V) = \nu_0 + aV + bV^3 + a\frac{b_V}{a_V}V^2 + \mathcal{O}((b_V/a_V)^2)$, and results in shifts up to 0.2 kHz, which we take as an additional uncertainty. We assume the offset and nonlinearity of the photodiode are uncorrelated and assign a net uncertainty of 0.32 kHz for photodiode imperfections.

I. Incoherent line-pulling

Nearby atomic resonances can pull the resonance frequency of interest. Transitions to the $8D_{3/2}$ state are the closest (57.13 MHz) that can contribute. The $2S_{1/2}-8D_{3/2}$ transition has a smaller matrix element than the $2S_{1/2}-8D_{5/2}$ transition, but for this upper bound we assume that they are equal. We estimate this effect by fitting a single Lorentzian to a pair of Lorentzians separated by 57.13 MHz and find a shift of less than 1 Hz, which is negligible.

J. Light-force shift

Metastable atoms traversing the 778 nm intensity profile are deflected from straight-line trajectories due to the AC Stark shift of the $|2S\rangle$ state. The energy shift of the $|2S\rangle$ state is given by

$$\Delta E(2S) = h \beta_{ac}(2S) I(\vec{r}), \quad (34)$$

where β_{ac} is the AC Stark shift coefficient [6], and $I(\vec{r})$ is the spatially varying intensity seen by the atom. The nonzero gradient of $I(\vec{r})$ produces a force which can deflect the atom to a region of differing AC Stark shift. We estimate an upper bound for the possible deflection, given as $\delta\vec{r}$, by considering the atom to be under a constant acceleration, which is found by assuming the maximal possible gradient of I for a given power, during the transit time. This can be estimated as

$$\delta\vec{r} \leq \frac{h}{2m} \beta_{ac}(2S) \nabla I|_{\max} (\Delta t)^2. \quad (35)$$

For 50 W in a Gaussian beam with a beam diameter of 600 μm , this corresponds to a maximal deflection of ~ 10 nm. This can correspond to an intensity variation of 10 ppm at most, which could vary the resulting AC Stark shift by a few Hz at the largest intensities. This effect is negligible at our current level of precision.

III. EFFECT OF AN ADDITIONAL YUKAWA POTENTIAL ON THE RYDBERG CONSTANT EXTRACTIONS

Here we discuss the effect of an additional perturbative potential of the form

$$V(r) = \beta \frac{e^{-r/\alpha}}{r}, \quad (36)$$

on the extraction of the Rydberg constant in hydrogen spectroscopy [20]. Here, β is the effective strength of the potential, and α gives the length scale. Following the discussion in [20], we allow for the sign of β to be both positive and negative.

We use first-order perturbation theory to calculate the effect of this perturbing potential on the hydrogen energy levels, given by $\delta E(n, l)$. The effect of this perturbation on an extraction of the Rydberg energy, $Ry = hcR_\infty$, from a specific measured transition is then

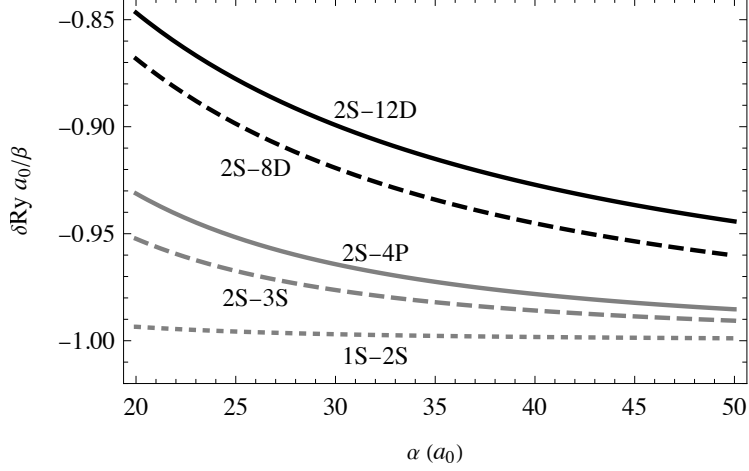


FIG. 5. Change in the extracted Rydberg energy due to a perturbing Yukawa potential (in units of β/a_0) as a function of the length scale α . 1S-2S: dotted grey, 2S-3S: dashed grey, 2S-4P: solid grey, 2S-8D: dashed black, 2S-12D solid black.

given by

$$\frac{\delta Ry}{Ry} = \frac{\delta E(n_2, l_2) - \delta E(n_1, l_1)}{E(n_2, l_2) - E(n_1, l_1)}, \quad (37)$$

where $E(n, l)$ is the energy of an unperturbed energy level and the subscripts 2 and 1 indicate the upper and lower states respectively, and δRy is the change in the Rydberg energy

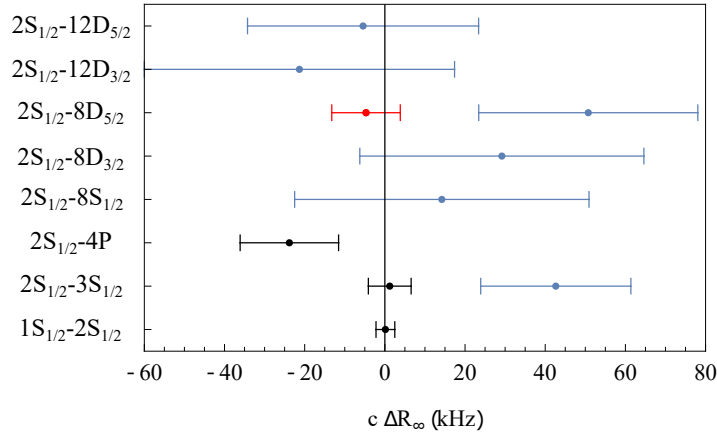


FIG. 6. Variation of Rydberg constant extractions from the weighted mean for the measured transitions shown in Fig. 5 of the main text but with the addition of the Yukawa potential perturbation. For this example, the length scale of the Yukawa potential is $\alpha = 34 a_0$ and $\beta = 1.64 \times 10^{-10} Ry a_0$. Blue points were measured in Paris (2S-3S [21], 2S-8S/D [23], 2S-12D [4]), black points were measured in Garching ($1S_{1/2}-2S_{1/2}$ [26], $2S_{1/2}-3S_{1/2}$ [25], 2S-4P [24]), and our result is in red.

determination. In Fig. 5, we show, δRy , scaled by β/a_0 as a function of the length scale α . As can be seen, the perturbation generally gives a larger Rydberg constant extraction as n_2 and n_1 increase provided that β is positive.

By considering an example length scale of $\alpha = 34 a_0$, where a_0 is the Bohr radius, and by scaling the effective strength of the potential to $\beta = 1.64 \times 10^{-10} Ry a_0$, the tension in the extractions of the Rydberg constant through hydrogen laser spectroscopy can be significantly reduced. This result is shown in Fig. 6. The extractions with this example Yukawa potential perturbation have a reduced chi-squared statistic of 2.0 while the data shown in Fig. 5 of the main text has a reduced chi-squared statistic of 4.0.

-
- [1] A. Beyer, L. Maisenbacher, A. Matveev, R. Pohl, K. Khabarova, A. Grinin, T. Lamour, D. C. Yost, T. W. Hänsch, N. Kolachevsky, T. Udem, The Rydberg constant and proton size from atomic hydrogen, *Science* **358**, 79 (2017).
 - [2] A. Grinin, A. Matveev, D. C. Yost, L. Maisenbacher, V. Wirthl, R. Pohl, T. W. Hänsch, T. Udem, Two-photon frequency comb spectroscopy of atomic hydrogen, *Science* **370**, 1061 (2020).
 - [3] H. Fleurbaey, S. Galtier, S. Thomas, M. Bonnaud, L. Julien, F. Biraben, F. Nez, M. Abgrall, J. Guéna, New Measurement of the 1S-3S Transition Frequency of Hydrogen: Contribution to the Proton Charge Radius Puzzle, *Phys. Rev. Lett.* **120**, 183001 (2018).
 - [4] B. De Beauvoir, C. Schwob, O. Acef, L. Jozefowski, L. Hilico, F. Nez, L. Julien, A. Clairon, F. Biraben, Metrology of the hydrogen and deuterium atoms: Determination of the Rydberg constant and Lamb shifts, *Eur. Phys. J. D* **12**, 61 (2000).
 - [5] A. E. Kramida, A critical compilation of experimental data on spectral lines and energy levels of hydrogen, deuterium, and tritium, *At. Data Nucl. Data Tables* **96**, 586 (2010).
 - [6] M. Haas, U. D. Jentschura, C. H. Keitel, N. Kolachevsky, M. Herrmann, P. Fendel, M. Fischer, T. Udem, R. Holzwarth, T. W. Hänsch, M. O. Scully, G. S. Agarwal, Two-photon excitation dynamics in bound two-body Coulomb systems including ac Stark shift and ionization, *Phys. Rev. A - At. Mol. Opt. Phys.* **73**, 052501 (2006).
 - [7] S. F. Cooper, A. D. Brandt, C. Rasor, Z. Burkley, D. C. Yost, Cryogenic atomic hydrogen beam apparatus with velocity characterization, *Rev. Sci. Instrum.* **91**, 013201 (2020).

- [8] M. A. Lombardi, The Use of GPS Disciplined Oscillators as Primary Frequency Standards for Calibration and Metrology Laboratories, *NCSLI Meas.* **3**, 56 (2008).
- [9] J. W. Farley, W. H. Wing, Accurate calculation of dynamic Stark shifts and depopulation rates of Rydberg energy levels induced by blackbody radiation. Hydrogen, helium, and alkali-metal atoms, *Phys. Rev. A* **23**, 2397 (1981).
- [10] S. A. Clough, Y. Beers, G. P. Klein, L. S. Rothman, Dipole moment of water from Stark measurements of H₂O, HDO, and D₂O, *J. Chem. Phys.* **2254**, 2254 (1973).
- [11] J. Cooper, Broadening of isolated lines in the impact approximation using a density matrix formulation, *Rev. Mod. Phys.* **39**, 167 (1967).
- [12] A. Matveev, N. Kolachevsky, C. M. Adhikari, U. D. Jentschura, Pressure shifts in high-precision hydrogen spectroscopy: II. Impact approximation and Monte-Carlo simulations, *J. Phys. B At. Mol. Opt. Phys.* **52**, 75006 (2019).
- [13] I. I. Sobel'man, *An Introduction to the Theory of Atomic Spectra* (Pergamon Press, 1972).
- [14] R. A. Swainson, G. W. F. Drake, A unified treatment of the non-relativistic and relativistic hydrogen atom: III. The reduced Green functions, *J. Phys. A. Math. Gen.* **24**, 1801 (1991).
- [15] H. A. Bethe, E. E. Salpeter, *Quantum Mechanics of One- and Two-Electron Atoms* (Springer-Verlag Berlin Heidelberg, New York, 1957), first edn.
- [16] M. Horbatsch, E. A. Hessels, Shifts from a distant neighboring resonance, *Phys. Rev. A - At. Mol. Opt. Phys.* **82**, 22513 (2010).
- [17] D. C. Yost, A. Matveev, E. Peters, A. Beyer, T. W. Hänsch, T. Udem, Quantum interference in two-photon frequency-comb spectroscopy, *Phys. Rev. A - At. Mol. Opt. Phys.* **90**, 012512 (2014).
- [18] H. Fleurbaey, F. Biraben, L. Julien, J. P. Karr, F. Nez, Cross-damping effects in 1S-3S spectroscopy of hydrogen and deuterium, *Phys. Rev. A* **95**, 52503 (2017).
- [19] T. Udem, L. Maisenbacher, A. Matveev, V. Andreev, A. Grinin, A. Beyer, N. Kolachevsky, R. Pohl, D. C. Yost, T. W. Hänsch, Quantum Interference Line Shifts of Broad Dipole-Allowed Transitions, *Ann. Phys.* **531**, 1900044 (2019).
- [20] M. P. A. Jones, R. M. Potvliege, M. Spannowsky, Probing new physics using Rydberg states of atomic hydrogen, *Phys. Rev. Res.* **2**, 013244 (2020).
- [21] H. Fleurbaey, S. Galtier, S. Thomas, M. Bonnaud, L. Julien, F. Biraben, F. Nez, M. Abgrall, J. Guéna, New Measurement of the 1S-3S Transition Frequency of Hydrogen: Contribution

- to the Proton Charge Radius Puzzle, *Phys. Rev. Lett.* **120**, 183001 (2018).
- [22] C. Schwob, L. Jozefowski, B. De Beauvoir, L. Hilico, F. Nez, L. Julien, F. Biraben, O. Acef, A. Clairon, Optical frequency measurement of the 2S-12D transitions in hydrogen and deuterium: Rydberg constant and lamb shift determinations, *Phys. Rev. Lett.* **82**, 4960 (1999).
- [23] B. De Beauvoir, F. Nez, L. Julien, B. Cagnac, F. Biraben, D. Touahri, L. Hilico, O. Acef, A. Clairon, J. J. Zondy, Absolute frequency measurement of the 2S-8S/D transitions in hydrogen and deuterium: New determination of the rydberg constant, *Phys. Rev. Lett.* **78**, 440 (1997).
- [24] A. Beyer, L. Maisenbacher, A. Matveev, R. Pohl, K. Khabarova, A. Grinin, T. Lamour, D. C. Yost, T. W. Hänsch, N. Kolachevsky, T. Udem, The Rydberg constant and proton size from atomic hydrogen, *Science* **358**, 79 (2017).
- [25] A. Grinin, A. Matveev, D. C. Yost, L. Maisenbacher, V. Wirthl, R. Pohl, T. W. Hänsch, T. Udem, Two-photon frequency comb spectroscopy of atomic hydrogen, *Science* **370**, 1061 (2020).
- [26] C. G. Parthey, A. Matveev, J. Alnis, B. Bernhardt, A. Beyer, R. Holzwarth, A. Maistrou, R. Pohl, K. Predehl, T. Udem, T. Wilken, N. Kolachevsky, M. Abgrall, D. Rovera, C. Salomon, P. Laurent, T. W. Hänsch, Improved Measurement of the Hydrogen 1S-2S Transition Frequency, *Phys. Rev. Lett.* **107**, 203001 (2011).